Pragya Darsan, 2025, 7(1) *@DEPAN, UCU*
ISSN: 2542-2634 (print) *Research Article*
https://doi.org/10.3126/pdmdj.v7i1.79765

CALCULATION OF ADSORPTION FREE ENERGY OF AROMATIC COMPOUNDS ON GRAPHENE SURFACE: A MOLECULAR DYNAMIC STUDY

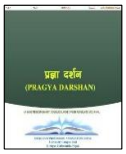

Gopi Chandra Kaphle[*1,2], Prabin Khadka[*1,2], Khemraj Bhatta[1,2], Binod Bhatta[1,2], Dhurba Prasad Acharya[2], Pradeep Bhujel[1], Mukunda KC[2], Dasu Ram Paudel[3]

[1]Department of Physics, GoldenGate Int' College, Devkota Road, Kathmandu, 44600, Bagmati, Nepal.
[2]Central Department of Physics, Tribhuvan University, Kirtipur Road, Kirtipur, 44600, Bagmati, Nepal.
[3]Department of Chemistry, Tri-Chandra Multiple Campus, Tribhuvan University, Kathmandu 44600, Nepal
Corresponding authors: gck223@gmail.com, prabinkhadka06@gmail.com

Received: January 10, 2025 Revised: March 13, 2025 Accepted: April 28, 2025

Abstract

Computational simulation techniques have become increasingly powerful and widespread due to advancements in computing capabilities which provide valuable insights into the behavior, properties, and interactions of nanoscale systems to accelerate development, optimize designs, and improve the safety and efficacy of nanomaterial-based applications. In the current study, adsorption equilibrium coefficients and free energy of some aromatic acids are calculated at different temperatures using molecular dynamics simulation along with free energy calculation to investigate the adsorption behavior of aromatic acid on graphene surface with temperature. The effect of temperature on the adsorption behavior of certain aromatic acids salicylic acid, benzoic acid, and phthalic acid- on carbon nanotubes was investigated using molecular dynamics simulation and free energy calculations at three different temperatures 260K, 300K, and 340K. Current analysis show that, in all temperature, salicylic acid has the highest adsorption and phthalic acid has the lowest (phthalic acid < benzoic acid < salicylic acid). It is discovered that the number of carboxylic acids that adsorb on carbon nanotubes increases with temperature.

Keywords*: carbon nanotube, aromatic compounds, free energy calculation, adsorption equilibrium constant*

Introduction

Graphene is a single atomic layer of hexagonally linked carbon atoms that exhibits a real two-dimensional (2D) crystalline structure and unique properties. The unique properties of the pristine graphene sheet, such as the theoretical specific surface area of thermal conductivity of $\sim 5000 W m^{-1} K^{-1}$, theoretical specific surface area $\sim 2630 m^2 g^{-1}$, Young's modulus of $\sim 0.1\, TPa$, good optical transmittance of ~97.7%, And intrinsic mobility of $\sim 2 \times 10^5\, cm^2 V^{-1} S^{-1}$, Graphene and its related mate- rials have strong potentials for a variety of applications over a broad wavelength range (Zhang et al., 2013). Fullerenes, nanotubes, nanodiamonds, and graphene are examples of carbon- based materials that are important for biomedical applications. Due to their high biocompatibility, fullerenes, graphene, and their derivatives are desirable candidates for biomedical applications, particularly in the fields of biosensing, imaging, and drug delivery (Navya & Daima, 2016).

Graphene-based nanocomposites have been widely used in numerous applications, including wound dressing (He et al., 2012; Liu et al., 2014; B. Lu et al., 2012; Madhavan et al., 2013), tissue engineering scaffolds (Faghihi et al., 2014; Mazaheri et al., 2014; Si et al., 2014) , water purification (Bao et al., 2011; Kumar et al., 2013; Musico et al., 2014), fabrication of antibacterial paper (Bao et al., 2011; W. Hu et al., 2010; Park et al., 2010; Sreeprasad et al., 2011), drug delivery (Gao et al., 2011; Pandey et al., 2011), and contaminant removal (F. Lu & Astruc, 2020; S. Wang et al., 2013), because of their excellent physicochemical and inherent antibacterial qualities. Fan et al. prepared highly flexible, reusable, and foldable GO-based cotton fabrics showed excellent antibacterial activities with minimal skin irritation which were found to inactive > 90% bacteria (Zhao et al., 2013). CS-PVA nanofibers containing graphene, collagen-fibrin composite film with GO (Deepachitra et al., 2014), GO-Ag composites into the polymer hydrogel were prepared and shows excellent antibacterial activity and accelerated the wound healing as well as wound dressing (Fan et al., 2014). In gelatin composite hydrogel GO nanosheets can be used for tissue engineering as a suitable scaffold, graphene-Ag nanowires, and GO-PVK nano composites have also been used as antibacterial coating (Kholmanov et al., 2012; Santos et al., 2011, 2012). Because of the properties such as high aspect ratio, rich surface chemistry, and ability to cross the plasma membrane, graphene has been widely used as an effective nanocarrier to deliver drugs such as antibiotics. The GO-PSA composite showed a significant increase in effective release time compared to the pure polysebacic anhydride (PSA) in releasing antibacterial drug levofloxacin (Gao et al., 2011). The GO-benzylpenicilin anion shows highly extended-release time and helps in enhancing synergistic antibacterial effect on GO

(Y. Wang et al., 2012). Sun et al. prepared a GO-balofloxacin nanocomposite and investigated the loading and release behavior of balofloxacin. The as-prepared nanocomposite exhibited a longer release time because of the hydrogen bonding interaction, which led to an excellent effect against E. coli (Li et al., 2013). Nafisi et al. systematically investigated the adsorption behavior of tetracycline onto GO at various pH, temperatures, and sorption times (Chand et al., 2021; Ghadim et al., 2013). Zhou et al. fabricated a carboxylate graphene-*β*-cyclodextrin/chlorhexidine acetate (GO-COOβ-CD/CA) inclusion as a graphene-based drug carrier. The inclusion showed great blood compatibility as indicated by hemolysis and the recalcification test. The inclusion also showed excel- lent antibacterial activity without any cytotoxic effect (Xiao et al., 2014).

Another important application of graphene with antibacterial properties is water purification. An rGO-Ag nanocomposite-modified porous carbon foam electrode was prepared by Kumar et al. to purify water. With the minimal power consumption of a 1.5-V battery, the antibacterial device can be used to rapidly purify drinking water (Kumar et al., 2013). Wang et al. prepared AgNPs and Ag@C on rGO and used them as electrodes in a capacitive deionization process to desalinate the seawater into drinking water (Cai et al., 2014). Ray et al. fabricated a nisin antibacterial peptide-conjugated 3D porous GO membrane for effective separation and inactivation of methicillin-resistant S. aureus (MRSA) pathogens from water (Kanchanapally et al., 2015). Graphene-based nanomaterial-modified membrane filters can be used in water treatment due to their enhanced antibacterial properties (Musico et al., 2014). Hyperbranched polyethylenimine (HPEI)-GO/polyethersulfone (PES) hybrid ultrafiltration membranes were fabricated via a classical phase inversion method by dispersing HPEI-modified GO in the PES casting solution. The as-prepared hybrid membranes exhibited excellent mechanical properties and good antibacterial activity, with potential applications beyond water purification or the fractionation of proteins and peptides (Yu et al., 2013). Bose et al. fabricated porous membranes for water purification by selectively etching one phase from a binary blend. Membranes decorated with rGO-Ag displayed enhanced synergistic bactericidal effect on E. coli (Kumar S Mural et al., 2015). Ruiz et al. used a GO nanomaterial as the filtration medium to eliminate bacteria from fuel. GO and GO-Ag columns could efficiently trap and inactive bacteria while allowing fuel to flow freely (Ruiz et al., 2015). Huang et al. fabricated a graphene-agarose hydrogel using agarose as the crosslinking agent and stabilizer. The as-prepared hydrogel showed remarkable antibacterial abil- ity, and it has been successfully fabricated into a gel column to purify miniature-scale water (Y. Wang et al., 2013). Very recently, an antibacterial rGO-Ag hydrogel composed of well-dispersed AgNPs and a porous rGO network was fabricated via a facile hydrothermal reaction for point-of-use water sterilization. The rGO network was used as the support for AgNPs, which in turn can facilitate the formation of the porous hydrogel. The bacte- ricidal filter composed of the rGO-Ag hydrogel showed good efficacy against E. coli. Moreover, the level of silver in the purified water was found to be much lower than the drinking water standard because silver is held by rGO (Zeng et al., 2015).

In recent years, molecular dynamics simulation with atomistic models and explicit sol- vent has been applied to elucidate interactions between common nanomaterials and organic molecules. Molecular dynamics simulation were employed to understand the adsorption affinity of number of neutral organic pollutants (Y. Wang et al., 2018), small organic molecules (Comer, Chen, et al., 2015), protein (Kang et al., 2009) on a graphene and its derivatives. L. Xu and X. Yang uses molecular dynamics simulation to investigate the interaction of pyrene-ployethene glycol (Pu- PEG) with graphene (Xu & Yang, 2014). Comer et. al. performs molecular dynamics simulation along with free energy calculation to investigate the interaction of different small organic molecules on graphene, carbon nanotube and successfully design the atrazine-CNT composite for drug delivery (Comer, Chen, et al., 2015). R.R. Johnson et. al. employed large-scale replica exchange molecular dynamics (REMD) simulation to find minima corresponding to six distinct conformations of oligonucleotide with DNA-carbon nanotube hybrid (DNA- CN) (Johnson et al., 2009). In the current work, the center of mass of the first graphene layer and the adsorbate molecule are defined along the z-axis. By collecting sample forces, the potential of the mean force is estimated along this transition co-ordinate. The interaction between the adsorbate molecules and the graphene surface is represented using the CHARMM general force field. The system is solvated using the common TIP3P water model. In order to investigate the temperature dependence of the probe molecules on the graphene surface, we calculated the adsorption equilibrium constants of three different distinct aromatic acids, salicylic acid, phthalic acids, and benzoic acid, at three different temperatures, 260K, 300K, and 340K. We haven't yet discovered the experimental evidence of such compounds' adsorption coefficient, though.

Methods

Adsorption on carbon nanotube

Force field parameters are extremely important in molecular dynamics simulations which defines the mathematical equations that govern the inter-atomic interactions and determines the motion and behavior of the adsorbate molecules in the simulated environment. In this work, we have used CHARMM general force field which include parameters for bond lengths, bond angles, torsion angles, van der Waals interactions, and electrostatic interactions. The mathematical equation that governs the simulation is (Duan et al., 2003; MacKerell et al., 1998; Oostenbrink et al., 2004).

$$U(\vec{r}) = \sum U_{bounded}(\vec{r}) + \sum U_{unbounded}(\vec{r})$$

$$= \sum_{i}\sum_{j>1} \epsilon_{ij}\left[\left(\frac{Rmin_{ij}}{r_{ij}}\right)^{12} - \left(\frac{Rmin_{ij}}{r_{ij}}\right)^{6}\right] + \frac{q_i\, q_j}{\epsilon_r r_{ij}} + \sum_{bonds} k_b\,(b-b_0)^2 + \sum_{angles} k_\theta\,(\theta-\theta_0)^2$$

$$+ \sum_{dihedrals} k_\chi\,[1+\cos(\eta\chi-\delta)] + \sum_{impropers} k_{imp}\,(\phi-\phi_0)^2 \qquad \ldots(1)$$

Here, the first and second term of the above equation represents the potential due to van der Waals and electrostatic interactions respectively. The first term of vender Waals represents repulsive potential due to overlapping electron clouds between interacting atoms and the second term represents the attractive potential due to induced dipole interactions. The symbol r_{ij} represents the distance between two atoms i and j is called interatomic or intermolecular separation; ϵij represents LJ well-depth; while $Rmin_{ij}$ is the radius in the Lennard-Jones potential. The coulombs potential is expressed by second term of above equation where r is relative permittivity called dielectric constant. Also, q_i and $q_j$represents the charge for particles i and j respectively. Third term of above equation represents potential due to bond between atoms where, b is bond length, b_0 is equilibrium bond length, k_b is the bond force constant. The fourth term of the above equation represents potential due to angle where, k is the force constant, is the angle between atoms and o is equilibrium bond angle. The 4-body atom torsion angle is also known as dihedral angle potential, describes the angular spring between the planes formed by the left sided three atomic plane and right sided three atomic plane of consecutively bonded atoms is represented by fifth term of above equation where, k_χ is dihedral force constant, η is multiplicity and δ is phase angle. Sixth term represent potential due to improper angles where ϕ is improper angle, ϕ_0 is improper equilibrium angle, and k_{imp} is improper force constant.

The adsorption of small aromatic compounds on carbon nanotubes is a promising area of research with potential applications in various elds. Here, molecular dynamics simulation has been used to investigate the adsorption behavior of small aromatic compounds on carbon nanotubes. We modeled multi-wall carbon nanotube having inside diameter of 12nm and height of 2nm. We assigned 6-member aromatic ring to graphene specified by CHARMM General Force Field (CGen) which determines how the carbon nanotube interact with other atoms and with itself. The carbon nanotube with periodic boundary condition, pervades to entire xy-plane having effectively large surface area. Comer et. al. has validated that modelling four graphene layers compared to single graphene layer has only little effect on adsorption equilibrium constant K_i^{cal}. With this validation, in the present work, we modeled four-layer graphene sheet for reasonable representation of the realistic system. In addition, small adsorbate molecules were parameterized by CHARMM general force field (CGenFF). The stadard TIP3P water model was used for the solvation of the system. Temperature and pressure were controlled by Langevin thermostat and group-based Langevin piston respectively. Moreover, free energy calculation was performed with Adaptive Biasing Force (ABF) between $0.3 \leq z \leq 1.5\ nm$ using a single window and Potential of Mean Force (PMF) was calculated by collecting sample forces along the transition co-ordinate.

Theoretical link between experiment and simulation in calculating adsorption equilibrium constant

In the relevant tests, a vial holding a colloid of water and a known quantity of nanoparticle (nanotubes) is introduced with varying amounts of a number of tiny aromatic compounds. Solid phase microextraction and gas chromatography mass spectrometry are used to precisely measure the final concentration of the substance that was not adsorbed to the nanoparticles. As a result, an adsorption equilibrium constant provides a useful way to describe the adsorption affinity for a specific molecule,

$$K_i^{expt} = \frac{V(c_i^0 - c_i^{eq})}{mc_i^{eq}} = \frac{VN_{i:NP}^{eq}}{mN_i^{eq}} \quad \ldots(2)$$

where V is the volume of liquid inside the vial, m is the total mass of nanoparticles inside the vial. c_i^0 is the concentration of compound i there before it came into contact with the nanoparticles, c_i^{eq} is the concentration of free compound i that is still there after equilibrium has been reached. The equilibrium numbers of the molecule i that has been adsorbed to the nanoparticle and is still free in solution are $N_{i:NP}^{eq}$ and N_i^{eq} respectively. The surface density of adsorbed molecules is relatively low when the lowest concentration is considerd in the experiment. The diameter of the adsorbate molecules is much less than a typical distance between each molecule. Thus, the interactions among the adsorbates can be neglected. The ratio $\frac{N_{i:NP}^{eq}}{N_i^{eq}}$ in equation (2) can be determined from free-energy calculations.

$$\frac{N_{i:NP}^{eq}}{N_i^{eq}} = \frac{\int_{adr} dr \exp\left[-\beta\omega_i(r)\right]}{\int_{free} dr \exp\left[-\beta\omega_i(r)\right]} \quad \ldots(3)$$

where $\omega_i(r)$ is the potential of mean force, $\beta = (k_B T)^{-1}$ is the reciprocal thermal energy and the integrals in the denominator and numerator are over molecule positions, as a function of the three-dimensional position in the vial in the adsorbed and free regions of space. The positions of the adsorbed molecule from any nanoparticle are $\omega(r) = 0$. Assuming that the concentration of colloid is sufficiently dilute, the denominator of equation (2) can be approximated to V. We obtain the potential of mean force of compound i, $\omega_i^{cal}(z)$ as a function of the distance between the plane passing through centre of mass of the first graphene surface and centre of mass of adsorbates by performing free energy calculation. Given su cient sampling, $\omega_i^{cal}(z)$ incorporates any lateral variability in the adsorption affinity. Equation (2) can therefore be written

$$\frac{N_{i:NP}^{eq}}{N_i^{eq}} \approx \frac{N_{NP}A_{NP}}{V} \int_0^c dz \exp\left[-\beta\omega_i^{cal}(z)\right] \quad \ldots(4)$$

where N_{NP} is the number of nanoparticles in the vial, A_{NP} is the accessible surface area of each of the nanoparticles, and c is a cutoff distance which defines the adsorbed region. All definitions of the integration limit c yield identical K_i values for the systems considered here. Substituting equation (4) into equation (2) gives us a route to estimate the adsorption equilibrium constant from the simulations:

$$K_i cal = \frac{A_{NP}}{M_{NP}} \int_0^c dz \exp\left[-\beta\omega_i^{cal}(z)\right] \quad \ldots(5)$$

where $\mathrm{M_{NP}} = \frac{\mathrm{m}}{\mathrm{N_{NP}}}$ is the typical mass of a single nanoparticle. The specific surface area $\frac{\mathrm{A_{NP}}}{\mathrm{M_{NP}}} = 233\ \mathrm{m^2/g}$ is experimentally determined by the Brunauer-Emmett Teller method (Comer, Chen, et al., 2015).

Modeling of Multilayer Graphene

We initially constructed a four-layer graphene system in a hexagonal box by using Inorganic Builder Plugin in VMD setting the dimensions $D{:}\,12$(inside diameter of hex-box) and $Z{:}\,2$ (height of the hex-box) where the plugin assigns all the required bond lengths, bond angles and constructs the protein structure le for the multilayer graphene system within certain periodic boundary conditions. The structure of multi-layer graphene is observed with the help of Visual Molecular Dynamics (VMD) which reads the graphene.pdb le (i.e. Protein Data bank File) to display it in visual screen. We assign the center of mass of the graphene system to (0,0, -11) position. Then, we represent graphene atoms with the CHARMM General Force Field (CGenFF) (MacKerell et al., 1998) type for 6-member aromatic rings to determine the nature of the way of interaction of graphene atoms with other atoms and with itself in the system. This creates ready Graphene layer structure le and databank le (Poblete et al., 2017).

Modeling of adsorbate molecule

First, we need to have structure le in order to parameterize the interested solute molecules. For this purpose, mol format of interested molecules can be obtained from the ChemSpider database http://www.chemspider.com/. The mol format containing the structure of the molecules is converted to mol2 format by using OpenBabel software. After that, mol2 le is uploaded in ParamChem server http://www.cgen.paramchem.org. that assigns parameters for the compound based on analogies between well parameterized model compounds in the CGenFF library and the chosen compound to get output le which contains topology and parameters of the molecule. Saving such le in compatible format .str, we convert it into .psf file using VMD and assembled a final psf and pdb file. The serial numbers of the atoms of solute molecules and top layer of graphene, step number, values of collective variable, values of biasing forces

were assigned using VMD. The collective variable defined is distance-z variable which gives component of a vector along z axis (0,0,1) between two points that are centre of mass of the first layer of graphene and centre of mass of solute molecule (Poblete et al., 2017).

Molecular Dynamics Simulation

NAMD2.12 was used to carry out all molecular dynamics simulations for the system, including graphene nanomaterials and each aromatic compounds. The standard three site TIP3P water model was used for aqueous environment in all simulations (Alexiadis & Kassinos, 2008). The temperature was controlled by Langevin thermostat at 260K, 300K, and 340K for each aromatic adsorbate molecules (Soddemann et al., 2003). The pressure was maintained at 1.01325 bar by using group-based Langevin piston acted only along z-axis (Quigley & Probert, 2004). The particle mesh Ewald algorithm with maximum grid spacing of 1.2 Å was employed to compute the electrostatic interactions. Van der Waals forces were computed using modified 14 VDW parameters with smooth cutoff of $8 - 9$ Å. A multiple time stepping scheme was employed to integrate the equation of motion with time stepping of 4 and 2 fs for long and short-range interactions. Visual Molecular Dynamics (VMD) was used in modeling, visualization and analysis of the system (Poblete et al., 2017).

Free energy calculation

Free energy is an important thermodynamic quantity that is very helpful in studying thermodynamic properties, phase transitions and stable states under external conditions. In the present work, we perform free energy calculation for three different adsorbate molecules- salicylic acid, benzoic acid and phthalic acid- at three different temperatures 260K, 300K and 340K on graphene surface having same functional group (carboxylic acid). Transition coordinate- the distance between center of mass of adsorbate molecule and center of mass of first layer graphene along z-axis- was defined using the Colvar module of NAMD 2.10. Before free energy calculation, system underwent 10000 steps of energy minimization and 500000 steps of equilibration which took about 10-15 minute of simulation. After minimization and equilibrium run, free energy calculation was performed with Adaptive Biasing Force (ABF) using NAMD 2.10 which took about 2 days of continuous simulation on a single processor computer (Comer, Gumbart, et al., 2015; Darve & Pohorille, 2001; Hénin & Chipot, 2004). The calculation was performed in between 03 z 15 nm using a single window and potential of mean force (PMF) is calculated by collecting sample forces, along the transition co-ordinate, in bins of width 0.05 A (Poblete et al., 2017).

Results and Discussion

Adsorption of salicylic acid on carbon nanotube

Salicylic acid is a naturally occurring compound in many plants, including willow trees, from which it was first isolated. Today, salicylic acid is widely used in a variety of applications, including as a skin care ingredient, as an active pharmaceutical ingredient, and in the production of other chemicals (Oostenbrink et al., 2004). Salicylic acid has been explored for potential applications in nanomedicine such as targeted drug delivery (Arif, 2015), cancer treatment (Mohammadian et al., 2017), wound healing (Zou et al., 2023), anti-inflammatory therapy, etc. (Koo et al., 2006). In order to com- prehend adsorption behavior of salicylic acid on carbon nanotube, potential of mean force and free energy were calculated using molecular dynamics simulation followed by free energy calculation.

Figure 1 [(a), (b) and (c)] shows energy profile of salicylic acid on graphene surface at three different temperature 260K, 300K, and 340K respectively. The contribution due to different energy parameters such as bonds, angles, dihedrals, kinetic, potential, electrostatics, and van der Waals on energy of the system is illustrated in Figure (1) and explicitly tabulated in table (1). All the parameters contributing to the energy of the system increases with temperature however van der Waals interaction decreases with temperature. We notice that weaker van der Waals forces is due to less interactions between the molecules since we have considered sufficiently low density in our simulation. In other hand, the kinetic energy of the system with temperature is found to be directly proportional to temperature illustrated in table (4) that lead to an increase in the distance between neighboring molecules and thus decreases the van der Waals forces. More kinetic energy may lead to an increase the magnitude of the fluctuating dipoles that increases the van der Waals forces however, in our case, this effect is found to be negligible. As temperature rises, it is discovered that the depth of potential energy decreases.

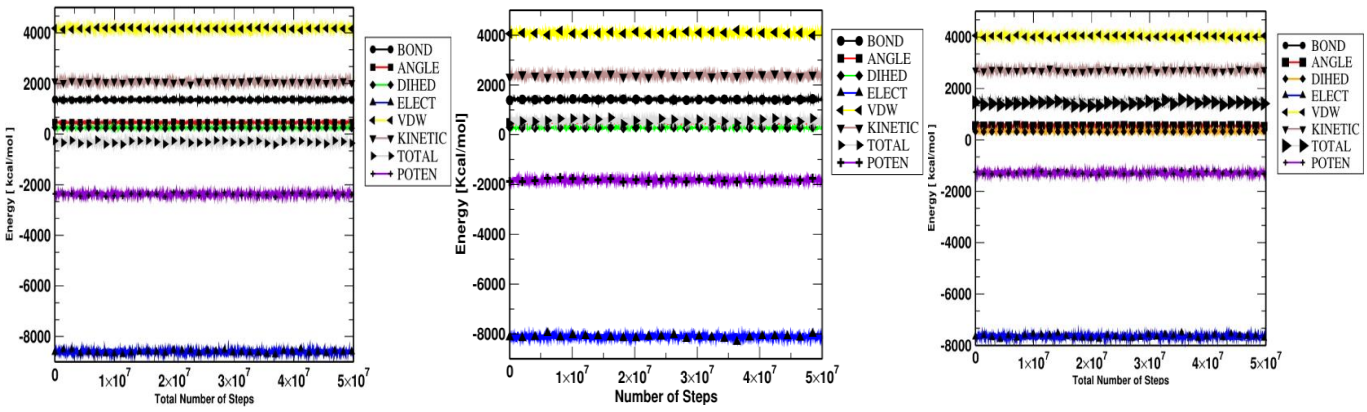

(a) **(b)** **(c)**

Figure 1: Energy profile of salicylic acid at (a) 260K (b) 300K (c) 340K

Table 1: Contribution of different energies at different temperatures of the system containing salicylic acid.

Energy (Kcal/Mol)	260K	300K	340K
Bond	1352.82 ± 0.46	1412.52 ± 0.54	1469.82 ± 0.61
Angle	455.53 ± 0.35	496.31 ±0.39	536.79 ±0.45
Proper dihedral	245.85± 0.42	283.28± 0.46	321.39± 0.56
Electrostatic	-8606.39± 2.35	-8120.34± 2.54	- 7652.59± 2.70
VDW	4166.47 ±1.52	4 091.57 ±1.60	4026.68 ±1.62
Potential	-2376.85 ±1.76	-1826.68± 1.94	- 1286.91± 2.19
Kinetic	2068.74 ±1.33	2389.95 ±1.55	2608.93 ±1.71
Total	-308.12 ±2.22	563.27 ±2.52	1422.02 ±2.76

Benzoic acid ($C_7H_6O_2$), melting point 122°C, is an aromatic carboxylic acid that is widely used in the food and pharmaceutical industries as a preservative (Hazan et al., 2004). Benzoic acid has been widely investigated for its potential applications. It has been used to modify the surface of nanoparticles such as gold and silver, to improve their stability and biocompatibility. It has been incorporated into various nanomaterials such as silver nanoparticles and graphene-oxide, to enhance their antimicrobial activity. In addition, it is used for imaging biological system, drug delivery and to improve drug loading capacity, (C.-M. J. Hu & Zhang, 2012; L. Wang et al., 2017; M. Wu et al., 2019; P. G. Wu & Brand, 1994) etc.

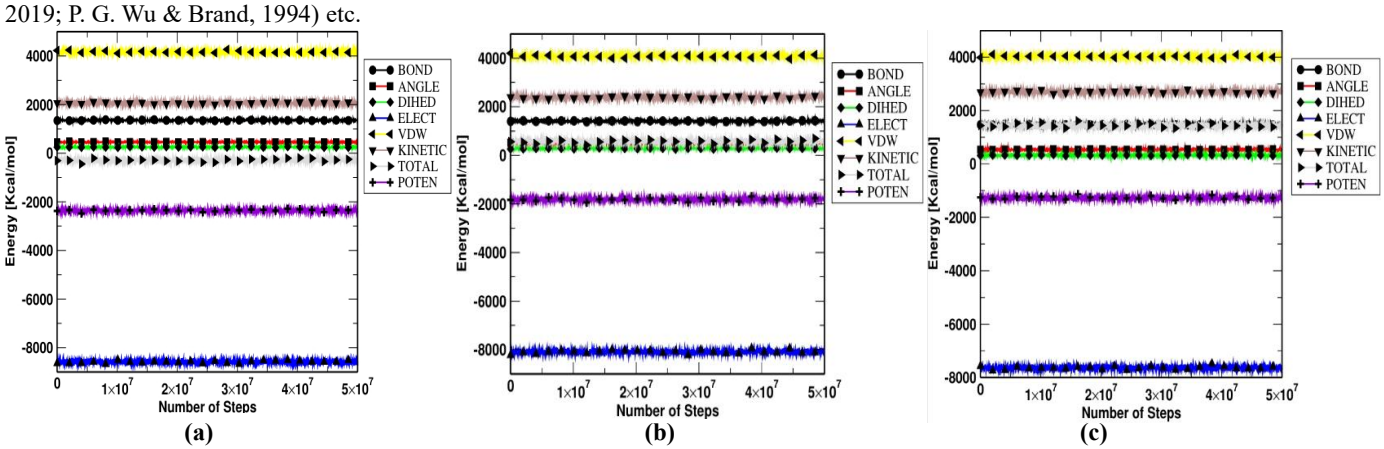

(a) **(b)** **(c)**

Figure 2: Energy profile of benzoic acid at (a) 260K (b) 300K (c) 340K

In order to comprehend adsorption behavior of benzoic acid on carbon nanotube, potential of mean force and free energy were calculated using molecular dynamics simulation followed by free energy calculation.

Figure 2[(a), (b) and (c)] shows energy profile of benzoic acid on graphene surface at three different temperature 260K, 300K, and 340K respectively. The contribution due to different energy parameters such as bonds, angles, dihedrals, kinetic, potential, electrostatics, and van der Waals on energy of the system is illustrated in Figure (2) and explicitly tabulated in table (2). According to the table (2), all sources of energy in the system increase as the system's temperature rises, with the exception of energy produced via van der Waal's interaction. When we examine kinetic energy, we see that kinetic energy is proportional with temperature explained in table (4). Depending on the simulation's temperature, potential and electrostatic energy is always negative, whereas total energy can either be positive or negative. Additionally, it is discovered that total energy increases with temperature.

Table 2: Contribution of different energies at different temperatures of the system containing benzoic acid.

Energy (Kcal/Mol)	260K	300K	340K
Bond	1352.05± 0.47	1410.33± 0.52	1468.65± 0.61
Angle	454.88 ±0.35	494.85±0.41	536.96 ±0.46
Proper dihedral	246.06± 0.42	284.47± 0.47	322.70± 0.54
Electrostatic	-8586.58± 2.42	-8096.41± 2.52	- 7642.57± 2.72
VDW	4165.81±1.56	4087.96 ±1.58	4027.97 ±1.64
Potential	-2358.91 ±1.77	-1808.63± 1.97	- 1277.32± 2.20
Kinetic	2069.39±1.32	2388.51 ±1.50	2709.07 ±1.73
Total	-289.52 ±2.21	579.88 ±2.52	1431.75 ±2.82

Phthalic acid $C_8H_6O_4$ is a white crystalline organic compound with melting point 191°*C*. Phthalic acid can form various salts and esters, which are widely used in the production of plastics, dyes, and pharmaceuticals (Abu Deiab et al., 2023). Phthalic acid has potential applications in carbon nanotube functionalization, Metal Organic Framework (MOFs), nanoparticle synthesis, anticancer agent, gene delivery, etc. (Huang et al., 2016; Ma et al., 2009). In order to comprehend adsorption behavior of phthalic acid on carbon nanotube, potential of mean force and free energy were calculated using molecular dynamics simulation followed by free energy calculation.

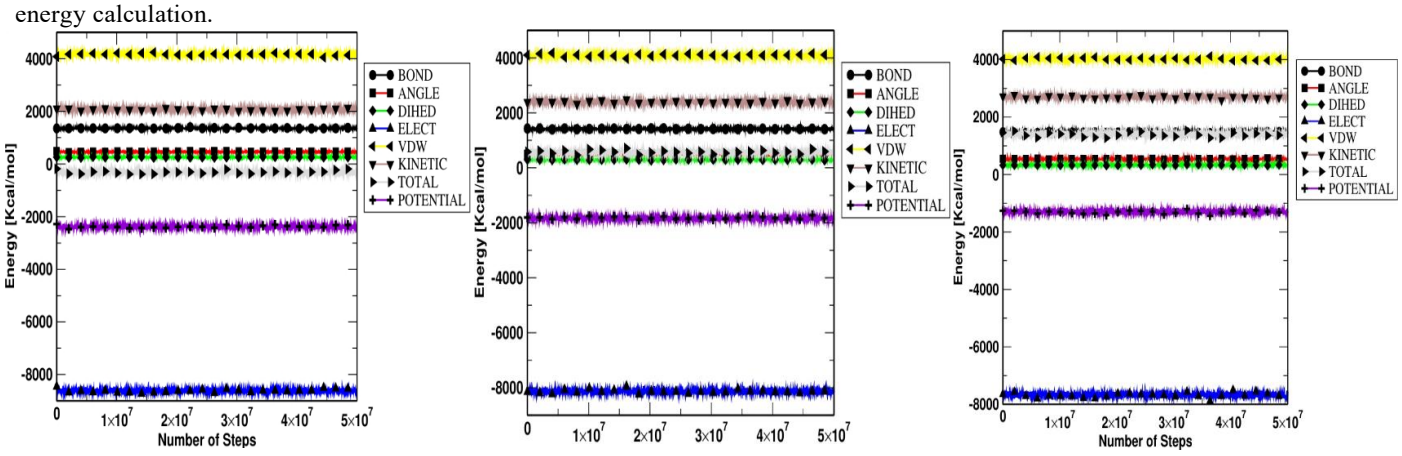

Figure 3: Energy profile of phthalic acid at (a) 260K (b) 300K (c) 340K

Figure 3[(a), (b) and (c)] shows energy profile of phthalic acid on graphene surface at three different temperature 260K, 300K, and 340K respectively. The contribution due to different energy parameters such as bonds, angles, dihedrals, kinetic, potential, electrostatics, and van der Waals on energy of the system is illustrated in Figure (3) and explicitly tabulated in Table (3). Table indicates that as the temperature of the system increases, all types of energy of the system increases except the energy contributed by van der Waal's interaction. As we look at kinetic energy, it shows that it grows as temperature. Electrostatic energy, potential energy as well as kinetic energy are increasing with temperature. Potential and electrostatic energy is always negative, and overall total energy may have positive or negative value depending on the temperature of simulation. In addition, total energy is found to be increasing with temperature. This shows that temperature is directly proportional to the total energy.

Table 3: Contribution of different energies at different temperatures of the system containing phthalic acid.

Energy (Kcal/Mol)	260K	300K	340K
Bond	1354.09± 0.47	1412.18± 0.53	1469.65± 0.61
Angle	455.94±0.36	496.58±0.41	536.99 ±0.47
Proper dihedral	254.56± 0.43	292.41± 0.49	329.03± 0.53
Electrostatic	-8621.65± 2.38	-8132.53± 2.52	- 7667.85± 2.77
VDW	4164.99±1.56	4089.36 ±1.61	4023.57 ±1.67
Potential	-2382.77 ±1.77	-1831.79± 1.96	- 1297.04± 2.26
Kinetic	2073.10±1.32	2390.16 ±1.49	2709.45 ±1.69
Total	-309.67 ±2.17	588.37 ±2.44	1412.41 ±2.84

Table 4: Variation of kinetic energy with temperature.

Temperature	Salicylic acid		Benzoic acid		Phthalic acid	
	K.E.	**K.E./T**	***K.E.***	**K.E./T**	***K.E.***	**K.E./T**
260K	2068.74±1.33	7.96	2069.39±1.31	7.96	2073.10±1.33	7.97
300K	2389.95±1.55	7.97	2388.51±1.50	7.96	2390.16±1.49	7.97
340K	2608.93±1.71	7.67	2709.07±1.73	7.97	2709.45±1.70	7.97

Binding energy of salicylic acid

The adsorption free energy curve of salicylic acid on the surface of the graphene layer at 260K, 300K, and 340K is shown in Figure 4.

From Figure 4, it can be inferred that at a distance $z < 3.0$ Å, there is no effect of binding of Salicylic acid on graphene. Above the distance $z \geq 3.0$ Å, the depth of the curve was increased, and lowest minima were attained at $z = 3.40$ Å, 3.45 Å and $z = 3.45$ Å for 260K, 300K and 340K respectively. We can infer that near $z = 3.45$ Å, there has been proper and maximum interaction between the salicylic acid and graphene layer Table 2 provides a summary of the free energy values at 260K, 300K, and 340K, which are -7.58Kcal mol^{-1}, -8.39Kcal mol^{-1}, and -8.66 Kcal mol^{-1} respectively. Additionally, after a constant value of $z = 10.00$ Å, the interaction between the surface of graphene and salicylic acid becomes insignificant, producing minute fluctuations. From table (5), we deduce that as the temperature of the system increases, its free energy also increases.

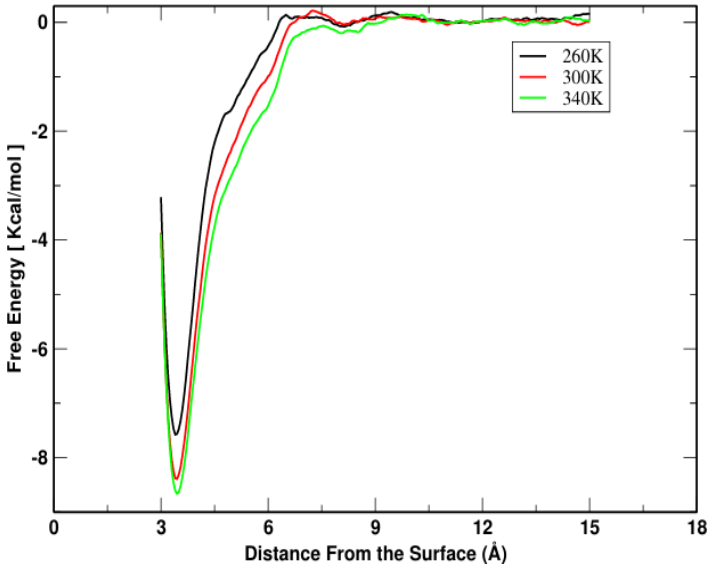

Figure 4: Adsorption free energy of salicylic acid on graphene surface at 260K, 300K and 340K

Binding energy of benzoic acid

The adsorption free energy curve of benzoic acid on the surface of the graphene layer at 260K, 300K, and 340K is shown in figure 5. We can deduce from figure 5 that there is no effect of binding of benzoic acid on graphene at a distance $z < 3.0$ Å. Above the distance $z \geq 3.0$ Å, the depth of the curve is increased, and lowest minima is attained at $z = 3.45$ Å,3.55 Å, and $z = 3.50$ Å for 260K, 300K, and 340K respectively. We infer that near $z = 3.45$ Å, there has been proper and maximum interaction between the benzoic acid and graphene layer, and the free energy values at 260K, 300K, and 340K are -6.88 Kcal mol^{-1}, -7.18 Kcal mol^{-1}, and -7.71 Kcal mol^{-1}, respectively. Additionally, after a constant value of $z = 3.45$ Å, the interaction between the surface of graphene and benzoic acid becomes insignificant, producing minute fluctuations. From Table (5), we deduce that as the temperature of the system increases, its free energy also increases.

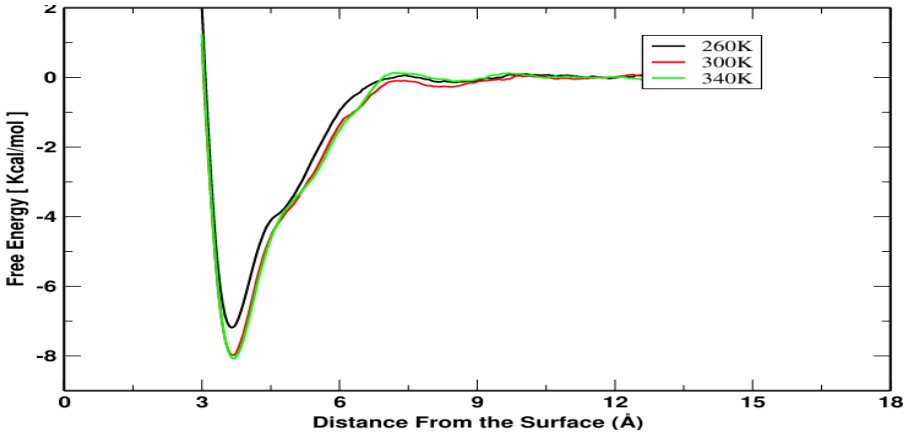

Figure 5: Adsorption free energy of benzoic acid on graphene surface at 260K, 300K and 340K

Binding energy of phthalic acid

The adsorption free energy curve of phthalic acid on the surface of graphene layer at 260K, 300K, and 340K is shown in Figure 6.

Figure 6 shows that there is no phthalic acid binding to graphene at a distance of $z < 3.0$ Å. The depth of the curve increased above $z \geq 3.0$ Å, and the lowest minima for 260K, 300K, and 340K, respectively, were achieved at $z = 3.65$ Å, $z = 3.70$ Å, and $z = 3.70$ Å. This indicates that near $z = 3.70$ Å, there has been proper and maximum interaction between the phthalic acid and the graphene layer. The free energy values at 260K, 300K, and 340K are -7.19 Kcal mol^{-1}, -7.89 Kcal mol^{-1}, and -8.80Kcal mol^{-1}, respectively.

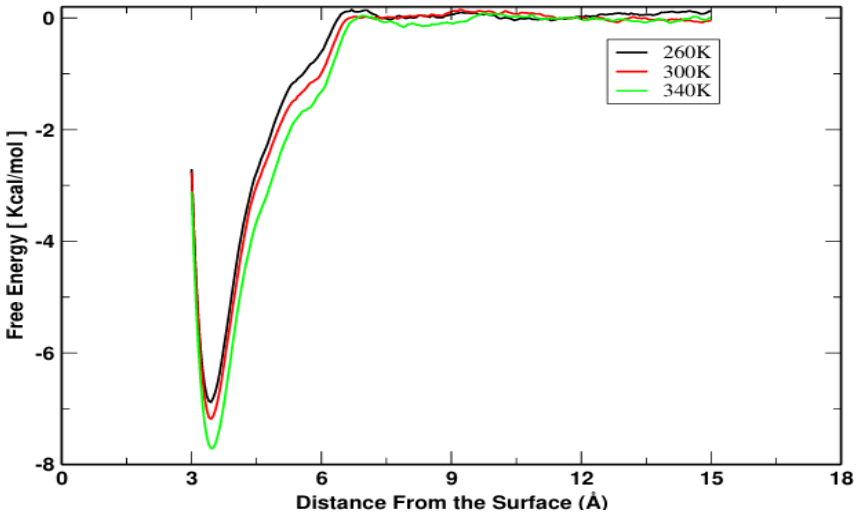

Figure 6: Adsorption free energy of phthalic acid on graphene surface at 260K, 300K, and 340K

Additionally, after a constant value of $z = 10.25$ Å, the interaction between the surface of graphene and phthalic acid becomes insignificant, producing minute fluctuations. From table (5), we deduce that as the temperatures of the system increases, its free energy also increases.

Table 5: Minimum free energy of certain aromatic acids at different temperatures.

Temperature	Salicylic acid		Benzoic acid		Phthalic acid	
	D.F.S.[1] (Å)	Free energy	D.F.S.[1] (Å)	Free energy	D.F.S.[1] (Å)	Free energy
260K	3.40	-7.85	3.45	-6.88	3.65	-7.19
300K	3.45	-8.39	3.45	-7.18	3.70	-7.98
340K	3.45	-8.66	3.45	-7.71	3.70	-8.08

[1]D.F.S. represents distance from the first layer of graphene surface.

Adsorption equilibrium constant

Table 6 shows the logarithmic value of adsorption equilibrium constants of three different aromatic compounds on graphene surface at three different temperatures. From table (6), the value of $logK_i^{calc}$ is increasing with temperature for all adsorbate molecules. The maximum value of $logK_i^{calc}$ is found highest for salicylic acid and minimum for benzoic acid at all temperature.

Table 6: Comparison of calculated logarithmic values of adsorption equilibrium coefficients of different atomic acids on carbon nanotube at different temperature.

S.N.	Compounds	260K ($logK_{cal}$)	300K ($logK_{cal}$)	340K ($logK_{cal}$)
1	Salicylic acid	3.39	3.99	4.20
2	Benzoic acid	2.93	3.14	3.74
3	Phthalic acid	3.17	3.74	3.81

Conclusion

Salicylic acid, benzoic acid, and phthalic acid in particular have been studied for their temperature dependence on the adsorption on graphene surface using molecular dynamics simulation and free energy calculations. It is discovered that the number of aromatic acids that adsorb on carbon nanotubes increases with temperature. In all temperatures, salicylic acid has the highest adsorption and benzoic acid has the low est. We hope, the design of nanomedicine and nanomaterials, as well as their delivery, will all bene t from this fundamental insight. The difference between the results from the experiment and the calculations could be caused by a number of different variables. It is highly likely that some of the discrepancy results from flaws in the force eld and water model. Because of the very abrupt change in dielectric characteristics at the graphene-water interface-which is known to be a point of failure for fixed charge atomic models-some explicit consideration of electronic polarizability may be required. As the classical molecular dynamics approach is incapable of adequately describing quantum chemical systems, some of the discrepancy even be inherent to it. On the other hand, insufficient sampling may lead to biased or inaccurate results.

Acknowledgments:

This work was supported by a University Grants Commission, Nepal (UGC-Nepal), Grant No. MRS-77/78-S & T-99.

References

Abu Deiab, G., Popova, M., Bashatwah, R., Ardakani, A., Aldhirat, J., Ayyad, A., & Alebraheem, A. (2023). Pharmacy Students' Success with Organic Chemistry Reactions of Small versus Large Drug-like Molecules. *Journal of Chemical Education*, *100*(4), 1426–1433. https://doi.org/10.1021/acs.jchemed.2c00658

Alexiadis, A., & Kassinos, S. (2008). Molecular Simulation of Water in Carbon Nanotubes. *Chemical Reviews*, *108*(12), 5014–5034. https://doi.org/10.1021/cr078140f

Arif, T. (2015). Salicylic acid as a peeling agent: a comprehensive review. *Clinical, Cosmetic and Investigational Dermatology*, 455. https://doi.org/10.2147/CCID.S84765

Bao, Q., Zhang, D., & Qi, P. (2011). Synthesis and characterization of silver nanoparticle and graphene oxide nanosheet composites as a bactericidal agent for water disinfection. *Journal of Colloid and Interface Science*, *360*(2), 463–470. https://doi.org/10.1016/j.jcis.2011.05.009

Cai, P.-F., Su, C.-J., Chang, W.-T., Chang, F.-C., Peng, C.-Y., Sun, I.-W., Wei, Y.-L., Jou, C.-J., & Wang, H. P. (2014). Capacitive deionization of seawater effected by nano Ag and Ag@C on graphene. *Marine Pollution Bulletin*, *85*(2), 733–737. https://doi.org/10.1016/j.marpolbul.2014.05.020

Chand, A., Chand, P., Khatri, G. G., & Paudel, D. R. (2021). Enhanced Removal Efficiency of Arsenic and Copper from Aqueous Solution Using Activated Acorus calamus Based Adsorbent. *Chemical and Biochemical Engineering Quarterly*, *3*. https://doi.org/10.15255/CABEQ.2021.1943

Comer, J., Chen, R., Poblete, H., Vergara-Jaque, A., & Riviere, J. E. (2015). Predicting Adsorption Affinities of Small Molecules on Carbon Nanotubes Using Molecular Dynamics Simulation. *ACS Nano*, *9*(12), 11761–11774. https://doi.org/10.1021/acsnano.5b03592

Comer, J., Gumbart, J. C., Hénin, J., Lelièvre, T., Pohorille, A., & Chipot, C. (2015). The Adaptive Biasing Force Method: Everything You Always Wanted To Know but Were Afraid To Ask. *The Journal of Physical Chemistry B*, *119*(3), 1129–1151. https://doi.org/10.1021/jp506633n

Darve, E., & Pohorille, A. (2001). Calculating free energies using average force. *The Journal of Chemical Physics*, *115*(20), 9169–9183. https://doi.org/10.1063/1.1410978

Deepachitra, R., Ramnath, V., & Sastry, T. P. (2014). Graphene oxide incorporated collagen–fibrin biofilm as a wound dressing material. *RSC Adv.*, *4*(107), 62717–62727. https://doi.org/10.1039/C4RA10150B

Duan, Y., Wu, C., Chowdhury, S., Lee, M. C., Xiong, G., Zhang, W., Yang, R., Cieplak, P., Luo, R., Lee, T., Caldwell, J., Wang, J., & Kollman, P. (2003). A point-charge force field for molecular mechanics simulations of proteins based on condensed-phase quantum mechanical calculations. *Journal of Computational Chemistry*, *24*(16), 1999–2012. https://doi.org/10.1002/jcc.10349

Faghihi, S., Gheysour, M., Karimi, A., & Salarian, R. (2014). Fabrication and mechanical characterization of graphene oxide-reinforced poly (acrylic acid)/gelatin composite hydrogels. *Journal of Applied Physics*, *115*(8). https://doi.org/10.1063/1.4864153

Fan, Z., Liu, B., Wang, J., Zhang, S., Lin, Q., Gong, P., Ma, L., & Yang, S. (2014). A Novel Wound Dressing Based on Ag/Graphene Polymer Hydrogel: Effectively Kill Bacteria and Accelerate Wound Healing. *Advanced Functional Materials*, *24*(25), 3933–3943. https://doi.org/10.1002/adfm.201304202

Gao, J., Bao, F., Feng, L., Shen, K., Zhu, Q., Wang, D., Chen, T., Ma, R., & Yan, C. (2011). Functionalized graphene oxide modified polysebacic anhydride as drug carrier for levofloxacin controlled release. *RSC Advances*, *1*(9), 1737. https://doi.org/10.1039/c1ra00029b

Ghadim, E. E., Manouchehri, F., Soleimani, G., Hosseini, H., Kimiagar, S., & Nafisi, S. (2013). Adsorption Properties of Tetracycline onto Graphene Oxide: Equilibrium, Kinetic and Thermodynamic Studies. *PLoS ONE*, *8*(11), e79254. https://doi.org/10.1371/journal.pone.0079254

Hazan, R., Levine, A., & Abeliovich, H. (2004). Benzoic Acid, a Weak Organic Acid Food Preservative, Exerts Specific Effects on Intracellular Membrane Trafficking Pathways in Saccharomyces cerevisiae. *Applied and Environmental Microbiology*, *70*(8), 4449–4457. https://doi.org/10.1128/AEM.70.8.4449-4457.2004

He, Y., Zhang, N., Gong, Q., Qiu, H., Wang, W., Liu, Y., & Gao, J. (2012). Alginate/graphene oxide fibers with enhanced mechanical strength prepared by wet spinning. *Carbohydrate Polymers*, *88*(3), 1100–1108. https://doi.org/10.1016/j.carbpol.2012.01.071

Hénin, J., & Chipot, C. (2004). Overcoming free energy barriers using unconstrained molecular dynamics simulations. *The Journal of Chemical Physics*, *121*(7), 2904–2914. https://doi.org/10.1063/1.1773132

Hu, C.-M. J., & Zhang, L. (2012). Nanoparticle-based combination therapy toward overcoming drug resistance in cancer. *Biochemical Pharmacology*, *83*(8), 1104–1111. https://doi.org/10.1016/j.bcp.2012.01.008

Hu, W., Peng, C., Luo, W., Lv, M., Li, X., Li, D., Huang, Q., & Fan, C. (2010). Graphene-Based Antibacterial Paper. *ACS Nano*, *4*(7), 4317–4323. https://doi.org/10.1021/nn101097v

Huang, H., Wu, K., Khan, A., Jiang, Y., Ling, Z., Liu, P., Chen, Y., Tao, X., & Li, X. (2016). A novel Pseudomonas gessardii strain LZ-E simultaneously degrades naphthalene and reduces hexavalent chromium. *Bioresource Technology*, *207*, 370–378. https://doi.org/10.1016/j.biortech.2016.02.015

Johnson, R. R., Kohlmeyer, A., Johnson, A. T. C., & Klein, M. L. (2009). Free Energy Landscape of a DNA−Carbon Nanotube Hybrid Using Replica Exchange Molecular Dynamics. *Nano Letters*, *9*(2), 537–541. https://doi.org/10.1021/nl802645d

Kanchanapally, R., Viraka Nellore, B. P., Sinha, S. S., Pedraza, F., Jones, S. J., Pramanik, A., Chavva, S. R., Tchounwou, C., Shi, Y., Vangara, A., Sardar, D., & Ray, P. C. (2015). Antimicrobial peptide-conjugated graphene oxide membrane for efficient removal and effective killing of multiple drug resistant bacteria. *RSC Advances*, *5*(24), 18881–18887. https://doi.org/10.1039/C5RA01321F

Kang, Y., Liu, Y.-C., Wang, Q., Shen, J.-W., Wu, T., & Guan, W.-J. (2009). On the spontaneous encapsulation of proteins in carbon nanotubes. *Biomaterials*, *30*(14), 2807–2815. https://doi.org/10.1016/j.biomaterials.2009.01.024

Kholmanov, I. N., Stoller, M. D., Edgeworth, J., Lee, W. H., Li, H., Lee, J., Barnhart, C., Potts, J. R., Piner, R., Akinwande, D., Barrick, J. E., & Ruoff, R. S. (2012). Nanostructured Hybrid Transparent Conductive Films with Antibacterial Properties. *ACS Nano*, *6*(6), 5157–5163. https://doi.org/10.1021/nn300852f

Koo, O. M. Y., Rubinstein, I., & Onyuksel, H. (2006). Camptothecin in Sterically Stabilized Phospholipid Nano-Micelles: A Novel Solvent pH Change Solubilization Method. *Journal of Nanoscience and Nanotechnology*, *6*(9), 2996–3000. https://doi.org/10.1166/jnn.2006.460

Kumar, S., Ghosh, S., Munichandraiah, N., & Vasan, H. N. (2013). 1.5 V battery driven reduced graphene oxide–silver nanostructure coated carbon foam (rGO–Ag–CF) for the purification of drinking water. *Nanotechnology*, *24*(23), 235101. https://doi.org/10.1088/0957-4484/24/23/235101

Kumar S Mural, P., Sharma, M., Shukla, A., Bhadra, S., Padmanabhan, B., Madras, G., & Bose, S. (2015). Porous membranes designed from bi-phasic polymeric blends containing silver decorated reduced graphene oxide synthesized via a facile one-pot approach. *RSC Advances*, *5*(41), 32441–32451. https://doi.org/10.1039/C5RA01656H

Li, F., Yang, C., Liu, B., & Sun, X. (2013). Properties of a Graphene Oxide-Balofloxacin Composite and Its Effect on Bacteriostasis. *Analytical Letters*, *46*(14), 2279–2289. https://doi.org/10.1080/00032719.2013.796557

Liu, Y., Park, M., Shin, H. K., Pant, B., Choi, J., Park, Y. W., Lee, J. Y., Park, S.-J., & Kim, H.-Y. (2014). Facile preparation and characterization of poly(vinyl alcohol)/chitosan/graphene oxide biocomposite nanofibers. *Journal of Industrial and Engineering Chemistry*, *20*(6), 4415–4420. https://doi.org/10.1016/j.jiec.2014.02.009

Lu, B., Li, T., Zhao, H., Li, X., Gao, C., Zhang, S., & Xie, E. (2012). Graphene-based composite materials beneficial to wound healing. *Nanoscale*, *4*(9), 2978. https://doi.org/10.1039/c2nr11958g

Lu, F., & Astruc, D. (2020). Nanocatalysts and other nanomaterials for water remediation from organic pollutants. *Coordination Chemistry Reviews*, *408*, 213180. https://doi.org/10.1016/j.ccr.2020.213180

Ma, L., Abney, C., & Lin, W. (2009). Enantioselective catalysis with homochiral metal–organic frameworks. *Chemical Society Reviews*, *38*(5), 1248. https://doi.org/10.1039/b807083k

MacKerell, A. D., Bashford, D., Bellott, M., Dunbrack, R. L., Evanseck, J. D., Field, M. J., Fischer, S., Gao, J., Guo, H., Ha, S., Joseph-McCarthy, D., Kuchnir, L., Kuczera, K., Lau, F. T. K., Mattos, C., Michnick, S., Ngo, T., Nguyen, D. T., Prodhom, B., … Karplus, M. (1998). All-Atom Empirical Potential for Molecular Modeling and Dynamics Studies of Proteins. *The Journal of Physical Chemistry B*, *102*(18), 3586–3616. https://doi.org/10.1021/jp973084f

Madhavan, A. A., Mohandas, A., Licciulli, A., Sanosh, K. P., Praveen, P., Jayakumar, R., Nair, S. V., Nair, A. S., & Balakrishnan, A. (2013). Electrospun continuous nanofibers based on a TiO2–ZnO–graphene composite. *RSC Advances*, *3*(47), 25312. https://doi.org/10.1039/c3ra44574g

Mazaheri, M., Akhavan, O., & Simchi, A. (2014). Flexible bactericidal graphene oxide–chitosan layers for stem cell proliferation. *Applied Surface Science*, *301*, 456–462. https://doi.org/10.1016/j.apsusc.2014.02.099

Mohammadian, F., Eatemadi, A., & Daraee, H. (2017). Inner ear drug delivery using liposomes. *Cellular and Molecular Biology*, *63*(1), 28. https://doi.org/10.14715/cmb/2017.63.1.6

Musico, Y. L. F., Santos, C. M., Dalida, M. L. P., & Rodrigues, D. F. (2014). Surface Modification of Membrane Filters Using Graphene and Graphene Oxide-Based Nanomaterials for Bacterial Inactivation and Removal. *ACS Sustainable Chemistry & Engineering*, *2*(7), 1559–1565. https://doi.org/10.1021/sc500044p

Navya, P. N., & Daima, H. K. (2016). Rational engineering of physicochemical properties of nanomaterials for biomedical applications with nanotoxicological perspectives. *Nano Convergence*, *3*(1), 1–14. https://doi.org/10.1186/s40580-016-0064-z

Oostenbrink, C., Villa, A., Mark, A. E., & Van Gunsteren, W. F. (2004). A biomolecular force field based on the free enthalpy of hydration and solvation: The GROMOS force-field parameter sets 53A5 and 53A6. *Journal of Computational Chemistry*, *25*(13), 1656–1676. https://doi.org/10.1002/jcc.20090

Pandey, H., Parashar, V., Parashar, R., Prakash, R., Ramteke, P. W., & Pandey, A. C. (2011). Controlled drug release characteristics and enhanced antibacterial effect of graphene nanosheets containing gentamicin sulfate. *Nanoscale*, *3*(10), 4104. https://doi.org/10.1039/c1nr10661a

Park, S., Mohanty, N., Suk, J. W., Nagaraja, A., An, J., Piner, R. D., Cai, W., Dreyer, D. R., Berry, V., & Ruoff, R. S. (2010). Biocompatible, robust free-standing paper composed of a TWEEN/graphene composite. *Advanced Materials*, *22*(15), 1736–1740. https://doi.org/10.1002/adma.200903611

Poblete, H., Miranda-Carvajal, I., & Comer, J. (2017). Determinants of Alanine Dipeptide Conformational Equilibria on Graphene and Hydroxylated Derivatives. *The Journal of Physical Chemistry B*, *121*(15), 3895–3907. https://doi.org/10.1021/acs.jpcb.7b01130

Quigley, D., & Probert, M. I. J. (2004). Langevin dynamics in constant pressure extended systems. *The Journal of Chemical Physics*, *120*(24), 11432–11441. https://doi.org/10.1063/1.1755657

Ruiz, O. N., Brown, N. A., Shiral Fernando, K. A., Harruff-Miller, B. A., Gunasekera, T. S., & Bunker, C. E. (2015). Graphene oxide-based nanofilters efficiently remove bacteria from fuel. *International Biodeterioration & Biodegradation*, *97*, 168–178. https://doi.org/10.1016/j.ibiod.2014.10.008

Santos, C. M., Mangadlao, J., Ahmed, F., Leon, A., Advincula, R. C., & Rodrigues, D. F. (2012). Graphene nanocomposite for biomedical applications: fabrication, antimicrobial and cytotoxic investigations. *Nanotechnology*, *23*(39), 395101. https://doi.org/10.1088/0957-4484/23/39/395101

Santos, C. M., Tria, M. C. R., Vergara, R. A. M. V., Ahmed, F., Advincula, R. C., & Rodrigues, D. F. (2011). Antimicrobial graphene polymer (PVK-GO) nanocomposite films. *Chemical Communications*, *47*(31), 8892. https://doi.org/10.1039/c1cc11877c

Si, H., Luo, H., Xiong, G., Yang, Z., Raman, S. R., Guo, R., & Wan, Y. (2014). One-Step In Situ Biosynthesis of Graphene Oxide–Bacterial Cellulose Nanocomposite Hydrogels. *Macromolecular Rapid Communications*, *35*(19), 1706–1711. https://doi.org/10.1002/marc.201400239

Soddemann, T., Dünweg, B., & Kremer, K. (2003). Dissipative particle dynamics: A useful thermostat for equilibrium and nonequilibrium molecular dynamics simulations. *Physical Review E*, *68*(4), 046702. https://doi.org/10.1103/PhysRevE.68.046702

Sreeprasad, T. S., Maliyekkal, M. S., Deepti, K., Chaudhari, K., Xavier, P. L., & Pradeep, T. (2011). Transparent, Luminescent, Antibacterial and Patternable Film Forming Composites of Graphene Oxide/Reduced Graphene Oxide. *ACS Applied Materials & Interfaces*, *3*(7), 2643–2654. https://doi.org/10.1021/am200447p

Wang, L., Hu, C., & Shao, L. (2017). The antimicrobial activity of nanoparticles: Present situation and prospects for the future. *International Journal of Nanomedicine*, *12*, 1227–1249. https://doi.org/10.2147/IJN.S121956

Wang, S., Sun, H., Ang, H. M., & Tadé, M. O. (2013). Adsorptive remediation of environmental pollutants using novel graphene-based nanomaterials. *Chemical Engineering Journal*, *226*, 336–347. https://doi.org/10.1016/j.cej.2013.04.070

Wang, Y., Comer, J., Chen, Z., Chen, J., & Gumbart, J. C. (2018). Exploring adsorption of neutral aromatic pollutants onto graphene nanomaterials via molecular dynamics simulations and theoretical linear solvation energy relationships. *Environmental Science: Nano*, *5*(9), 2117–2128. https://doi.org/10.1039/C8EN00575C

Wang, Y., Zhang, D., Bao, Q., Wu, J., & Wan, Y. (2012). Controlled drug release characteristics and enhanced antibacterial effect of graphene oxide–drug intercalated layered double hydroxide hybrid films. *Journal of Materials Chemistry*, *22*(43), 23106. https://doi.org/10.1039/c2jm35144g

Wang, Y., Zhang, P., Liu, C. F., & Huang, C. Z. (2013). A facile and green method to fabricate graphene-based multifunctional hydrogels for miniature-scale water purification. *RSC Advances*, *3*(24), 9240. https://doi.org/10.1039/c3ra22687e

Wu, M., Vartanian, A. M., Chong, G., Pandiakumar, A. K., Hamers, R. J., Hernandez, R., & Murphy, C. J. (2019). Solution NMR Analysis of Ligand Environment in Quaternary Ammonium-Terminated Self-Assembled Monolayers on Gold Nanoparticles: The Effect of Surface Curvature and Ligand Structure. *Journal of the American Chemical Society*, *141*(10), 4316–4327. https://doi.org/10.1021/jacs.8b11445

Wu, P. G., & Brand, L. (1994). Resonance Energy Transfer: Methods and Applications. *Analytical Biochemistry*, *218*(1), 1–13. https://doi.org/10.1006/abio.1994.1134

Xiao, Y., Fan, Y., Wang, W., Gu, H., Zhou, N., & Shen, J. (2014). Novel GO-COO-β-CD/CA inclusion: its blood compatibility, antibacterial property and drug delivery. *Drug Delivery*, *21*(5), 362–369. https://doi.org/10.3109/10717544.2013.846997

Xu, L., & Yang, X. (2014). Molecular dynamics simulation of adsorption of pyrene–polyethylene glycol onto graphene. *Journal of Colloid and Interface Science*, *418*, 66–73. https://doi.org/10.1016/j.jcis.2013.12.005

Yu, L., Zhang, Y., Zhang, B., Liu, J., Zhang, H., & Song, C. (2013). Preparation and characterization of HPEI-GO/PES ultrafiltration membrane with antifouling and antibacterial properties. *Journal of Membrane Science*, *447*, 452–462. https://doi.org/10.1016/j.memsci.2013.07.042

Zeng, X., McCarthy, D. T., Deletic, A., & Zhang, X. (2015). Silver/Reduced Graphene Oxide Hydrogel as Novel Bactericidal Filter for Point-of-Use Water Disinfection. *Advanced Functional Materials*, *25*(27), 4344–4351. https://doi.org/10.1002/adfm.201501454

Zhang, Y., Wu, C., Guo, S., & Zhang, J. (2013). Interactions of graphene and graphene oxide with proteins and peptides. *Nanotechnology Reviews*, *2*(1), 27–45. https://doi.org/10.1515/ntrev-2012-0078

Zhao, J., Deng, B., Lv, M., Li, J., Zhang, Y., Jiang, H., Peng, C., Li, J., Shi, J., Huang, Q., & Fan, C. (2013). Graphene Oxide-Based Antibacterial Cotton Fabrics. *Advanced Healthcare Materials*, *2*(9), 1259–1266. https://doi.org/10.1002/adhm.201200437

Zou, Y., Lu, N., Yang, X., Xie, Z., Lei, X., Liu, X., Li, Y., Huang, S., Tang, G., & Wang, Z. (2023). Synthesis and anti-hepatocellular carcinoma evaluation of salicylic acid-modified indole trimethoxy flavonoid derivatives. *RSC Medicinal Chemistry*, *14*(6), 1172–1185. https://doi.org/10.1039/D3MD00128H